Cell Reports
Article

Cell PRESS
Open ACCESS

Uncovering Scaling Laws to Infer Multidrug Response of Resistant Microbes and Cancer Cells

Kevin B. Wood,[1] Kris C. Wood,[2,3] Satoshi Nishida,[1] and Philippe Cluzel[1,*]
[1]FAS Center for Systems Biology, Department of Molecular and Cellular Biology, School of Engineering and Applied Sciences, Harvard University, 52 Oxford Street, Cambridge, MA 02138, USA
[2]Whitehead Institute for Biomedical Research, 9 Cambridge Center, Cambridge, MA 02142, USA
[3]Present address: Department of Pharmacology and Cancer Biology, Duke University School of Medicine, Durham, NC 27710, USA
*Correspondence: cluzel@mcb.harvard.edu
http://dx.doi.org/10.1016/j.celrep.2014.02.007

SUMMARY

Drug resistance in bacterial infections and cancers constitutes a major threat to human health. Treatments often include several interacting drugs, but even potent therapies can become ineffective in resistant mutants. Here, we simplify the picture of drug resistance by identifying scaling laws that unify the multidrug responses of drug-sensitive and -resistant cells. On the basis of these scaling relationships, we are able to infer the two-drug response of resistant mutants in previously unsampled regions of dosage space in clinically relevant microbes such as *E. coli*, *E. faecalis*, *S. aureus*, and *S. cerevisiae* as well as human non-small-cell lung cancer, melanoma, and breast cancer stem cells. Importantly, we find that scaling relations also apply across evolutionarily close strains. Finally, scaling allows one to rapidly identify new drug combinations and predict potent dosage regimes for targeting resistant mutants without any prior mechanistic knowledge about the specific resistance mechanism.

INTRODUCTION

Treatment strategies for infectious diseases and cancers often involve multiple drugs that must be combined, adapted, and refined to target evolving cell populations. Multidrug therapies can be difficult to design because drugs often interact, making their combined effects larger or smaller than expected from their individual effects (Bliss, 1956; Fitzgerald et al., 2006; Greco et al., 1995; Keith et al., 2005; Lehár et al., 2008; Loewe, 1953). Furthermore, well-developed multidrug treatments can be thwarted by the emergence of multidrug resistance, which arises in both bacterial infections and cancer, and represents a growing public health threat (Levy and Marshall, 2004). For example, potent drug regimens designed to target a particular cancer may be rendered ineffective by the rapid evolution of drug resistance (Garrett and Arteaga, 2011; Glickman and Sawyers, 2012; Poulikakos and Rosen, 2011). In addition, drugs may interact differently in each new resistant mutant, making the molecular characterization of resistance a time-consuming and at times untenable goal. Because of the rapidly increasing number of multidrug-resistant mutants, there is a significant need for new strategies to characterize and refine drug regimens in hopes of mitigating the effects of resistance.

Scaling laws can offer a complementary approach for simplifying the picture of multidrug-resistance without relying on highly time- and resource-consuming molecular studies. These laws, which can be surprisingly simple, are often based on symmetry arguments rather than system-specific microscopic details. Scaling is powerful because it offers a quantitative unifying framework for systems that appear, on the surface, to be very different. For example, allometric scaling laws (Shoval et al., 2012) connect anatomical and physiological features, such as body mass and metabolism, across a wide range of organisms. Similar relations have contributed to our understanding of phenotypic variability in populations of bacteria (Balaban et al., 2004) and eukaryotic immune cells (Feinerman et al., 2008), the fluctuation-response relationship in bacterial chemotaxis (Park et al., 2010), the structural properties of metabolic networks (Jeong et al., 2000), growth and gene expression in populations of *Escherichia coli* (Scott et al., 2010), and epistatic interactions between genes in yeast (Velenich and Gore, 2013). Motivated by the success of scaling laws across disciplines, we set out to identify similar principles that could unify the description of drug interactions in sensitive and resistant cells. The discovery of such scaling relations could provide an approach for systematically adapting multidrug treatments to effectively combat drug resistance, even before the molecular mechanisms have been fully elucidated.

RESULTS

Drug Interactions Can Change following Acquisition of Resistance

We first asked how acquired drug resistance affects the interactions between two drugs observed initially in wild-type (WT)

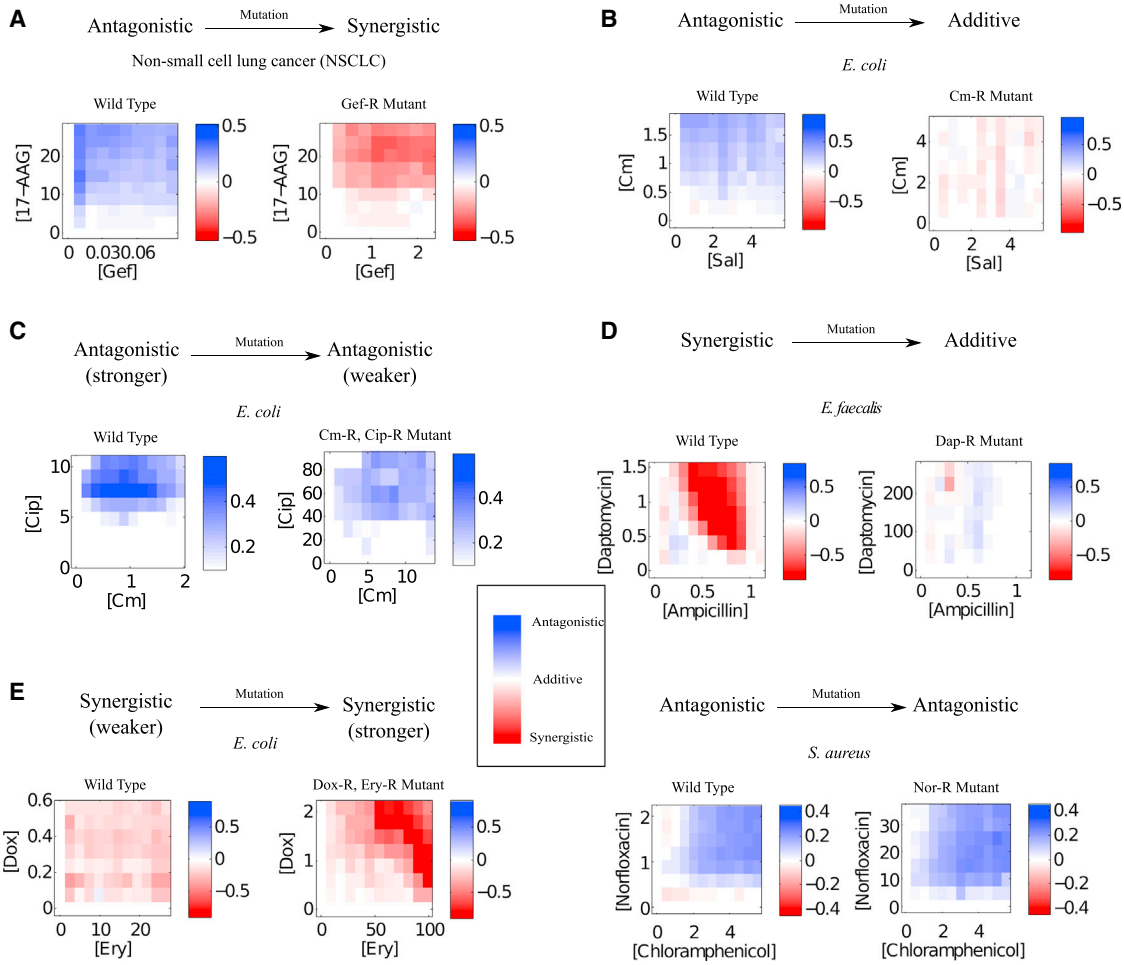

Figure 1. Resistance that Either Alters or Conserves Interactions between Drugs in Prokaryotic and Eukaryotic Cells

Heatmaps quantify the drug interaction and classify it as synergistic or antagonistic across a range of active concentrations for both WT and mutant cells. To quantify the drug interaction at each point on the response surface, we define the interaction parameter $I = \log_2(g_{12} - g_1\, g_2 + 1)$, which is positive (blue) for antagonistic, negative (red) for synergistic interactions (Bollenbach and Kishony, 2011), and zero when there is no interaction ($g_{12} = g_1\, g_2$, consistent with Bliss independence). In addition to modifying the resistance of cells to one or more drugs, resistance events can sometimes modify the interactions between drug pairs. See Figure S1 for an alternative quantification of drug interactions. We note that because the mutants in this study are resistant to at least one drug, we must use higher drug concentrations for the mutant cells to obtain growth reduction. However, we estimated the drug interactions over concentration ranges that yield approximately similar growth reductions in mutant and WT cells (Figure S1). Drug concentrations are given in units of μg/ml unless otherwise noted.

(A) Gefitinib (Gef) resistance in NSCLC cells changes the interaction between 17-AAG and gefitinib from strongly antagonistic (suppressive) to synergistic. [17-AAG] and [gefitinib] are in units of nM and μM, respectively.

(B) Chloramphenicol (Cm) resistance in *E. coli* changes the interaction between salicylate (Sal) and Cm from strongly antagonistic (suppressive) to additive/weakly synergistic.

(C) Cm and ciprofloxacin (Cip) resistance in *E. coli* weakens the strongly antagonistic (suppressive) interaction between Cm and Cip, but does not eliminate the antagonism. [Cip] is in units of ng/ml.

(D) Daptomycin (Dap) resistance in *E. faecalis* reduces the strongly synergistic interaction between ampicillin and Dap.

(E) Erythromycin (Ery) and doxycycline (Dox) resistance in *E. coli* increases the synergistic interaction between the two drugs.

(F) Norfloxacin (Nor) resistance in *S. aureus* does not change the interaction between Cm and Nor.

drug-sensitive cells. To answer this question, we measured the population growth of a wide range of organisms, including bacteria and human cancer cells, in response to drug pairs (Supplemental Experimental Procedures; Tables S1–S3). We then quantified the nature of the drug interaction, i.e., synergy or antagonism, in both WT and resistant cells using two standard pharmacology approaches (Figures 1 and S1). Interestingly, we find that resistance can alter not only the individual drug efficacies but also the interactions between drugs. That is, two drugs can interact quite differently depending on whether they are applied to drug-resistant mutants or drug-sensitive cells (Figures 1 and S1). For example, the combination of two anticancer agents, gefitinib and 17-AAG, is antagonistic for most dosages in *EGFR* mutant non-small-cell lung cancer (NSCLC) cells, making it an unlikely a priori choice for therapy (Figure 1A). However, the same drug pair becomes synergistic for most dosages (Xu et al.,

2012) in a gefitinib-resistant mutant (Engelman et al., 2007; Figure 1A). On the other hand, in *E. coli*, the antagonism between some drug pairs is eliminated (Figure 1B) or reduced (Figure 1C) in antibiotic-resistant mutants, but the interactions do not become synergistic. A similar decrease in the interactions between antibiotics occurs in vancomycin-resistant *Enterococcus faecalis* (Palmer et al., 2011), where the synergy (Rand and Houck, 2004) in the combination of daptomycin and ampicillin is reduced in certain daptomycin-resistant mutants (Figure 1D). By contrast, in *E. coli* exposed to the weakly synergistic combination of doxycycline (Dox) and erythromycin (Ery), the drug pair becomes increasingly synergistic in some multidrug-resistant mutants (Figure 1E). We also observe cases in which the drug interactions are not changed by resistance events. For example, the antibiotics chloramphenicol (Cm) and norfloxacin (Nor) show approximately the same level of antagonism in *Staphylococcus aureus* cells and Nor-resistant mutants. In this case, the mutation reduces the effective concentration at which Nor becomes toxic, but otherwise does not modify the shape of the cell's two-drug response surface. Similar results have been reported for some mutations in *E. coli* (Chait et al., 2007). In summary, we find that resistance can alter drug interactions in multiple different ways, and there is no obvious relationship between the interactions observed in sensitive cells and those in resistant mutants.

A Simple Model Can Describe a Wide Range of Two-Drug Response Surfaces

To establish a relationship between drug interactions before and after the acquisition of resistance, we constructed a simple model to quantitatively characterize growth response surfaces after exposure to two drugs (separately or in combination). Response surfaces are commonly used to quantify and classify the interactions between two drugs based on measurements of cell proliferation (Fitzgerald et al., 2006; Greco et al., 1995; Lehár et al., 2007, 2008). However, most models apply to only a subset of all measured response surfaces because they are based on simplified enzyme kinetics or are specific to particular drug classes and particular intracellular pathways (Fitzgerald et al., 2006; Greco et al., 1995; Lehár et al., 2007, 2008). To account for different types of response surfaces, we used a model of the following multiplicative form:

$$g_{1,2} = g_1(D_1)g_2(D_{2eff}) \qquad \text{(Equation 1)}$$

where $g_{1,2}$ is the growth in the presence of drugs 1 and 2 together, g_1 is the growth as a function of drug 1 alone, and g_2 is the growth as a function of drug 2 alone. D_1 is the concentration of drug 1, and D_{2eff} is the effective concentration of drug 2, which accounts for interactions between the drugs. Changing the concentration D_2 into D_{2eff} formally captures the interaction between the two drugs by allowing the presence of one drug (D_1) to modify the effective concentration and hence the toxicity of the other drug (D_2) according to

$$D_{2eff} = D_2(1 + C(D_1))^{-1}, \qquad \text{(Equation 2)}$$

Note that D_{2eff} is equal to the concentration D_2 modified by a factor $(1 + C(D_1))^{-1}$ that depends only on D_1. This dependence is governed by the function $C(D_1)$, which we call the two-drug toxicity function (see Supplemental Results). The specific definition of this factor is empirical and was chosen by analogy to simple efflux-mediated drug interactions (Wood and Cluzel, 2012). The function $C(D_1)$ will prove essential for establishing scaling relationships between WT and mutant cells. Importantly, Equations 1 and 2 allow us to decompose two-drug response surfaces into three simpler, one-dimensional "basis functions": $g_1(D_1)$, $g_2(D_2)$, and $C(D_1)$.

We first verified that this model is sufficiently general to describe, with a minimal number of parameters, all experimentally observed response surfaces. Figure 2A shows a typical example of a response surface, in this case for *E. coli*, in the presence of the antibiotics Cm and ciprofloxacin (Cip) (for experimental details, see Supplemental Experimental Procedures). Strongly antagonistic behavior between these drug classes has been linked with a suboptimal ratio of protein to DNA in the cell (Bollenbach et al., 2009). Using the measured two-dimensional response surface, we first extracted the one-drug toxicity functions (g_1 and g_2) and then determined the two-drug toxicity function $C(D_1)$ empirically from the data. Specifically, we fit the response surface data using the two latter equations and an empirical parameterization for $C(D_1)$. We selected the best parameterization of $C(D_1)$ among a set of 11 possibilities using Akaike Information Criteria, a robust model selection technique (Supplemental Results). Together with Equation 1, these three functions (g_1, g_2, and $C(D_1)$) determine the bacterial growth response surface for any concentration of the two drugs (Figure 2, right).

The model provides a similarly good description for all of the 19 additional drug pairs tested (Supplemental Results; Table S5), spanning a wide range of response surfaces and yielding $C(D_1)$ functions with many different shapes (Figure 2B). In some mechanistically tractable cases, the two-drug toxicity function is constrained by the intracellular molecular pathways underlying the single-drug and multidrug responses (Supplemental Results; Figure S2). For example, in the multiple antibiotic resistance (MAR) system, $C(D_1)$ is proportional to the activity of the mar promoter (Figure S2B; Wood and Cluzel, 2012). More generally, the model decomposes two-dimensional response surfaces into three simpler, empirical functions that do not require a detailed molecular understanding of the drug interaction or mode of action.

The Decomposition of Response Surfaces into Basis Functions Reveals Scaling Relationships between Drug-Sensitive and -Resistant Cells

Next, we exploited the decomposition of response surfaces into basis functions to search for mathematical relationships between the multidrug responses of drug-sensitive and -resistant cells. We hypothesized that certain properties of the basis functions should be conserved when bacteria become drug resistant. Specifically, we postulated that the effect of resistance could be to (1) rescale the concentration of each drug, with the scaling factors a_1 or a_2 being specific to each mutant, and/or (2) change the interaction between drugs by rescaling

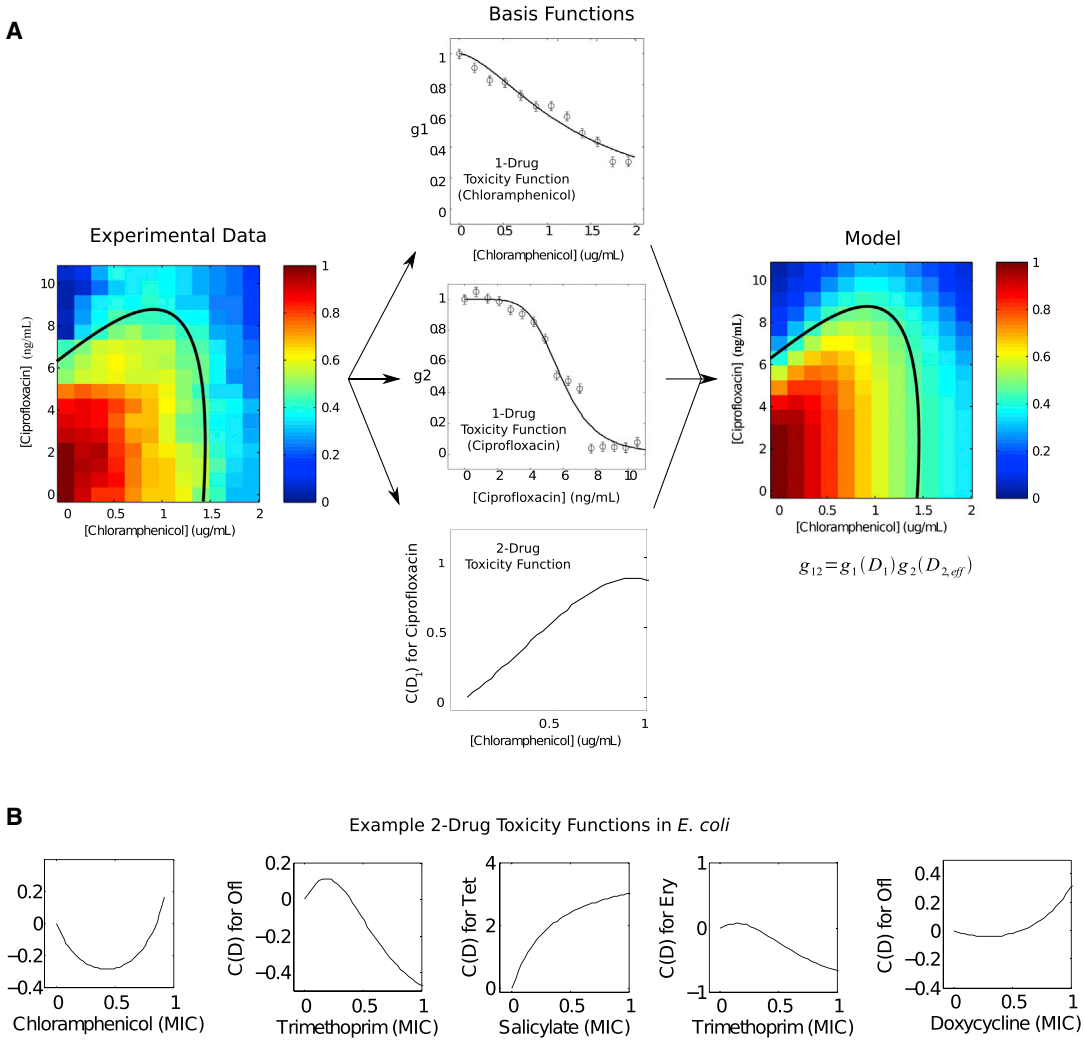

Figure 2. Characterization of Bacterial Response to a Pair of Drugs with a Set of Three Unique Basis Functions

(A) Experimental heatmap of growth rate relative to that of untreated cells in response to a pair of drugs (Cm and Cip, left). Red is maximum growth, blue is no growth. See Supplemental Experimental Procedures for an estimate of uncertainty in growth rate. [Cm] and [Cip] are in units of μg/ml and ng/ml, respectively. Drug 1 (Cm, middle top), drug 2 (Cip, middle center), and two-drug toxicity functions ($C(D_1)$, middle bottom) are shown. The one-drug toxicity functions are modeled using the Hill form, which is commonly used in pharmacology, where K_i is the concentration of drug i (for $i = 1,2$) at which the effect is half-maximal (also known as the IC_{50}), and n_i is the Hill coefficient describing the slope of the response. The function $C(D_1)$ is an empirically determined function that captures the effect of drug 1 (Cm) on drug 2 (Cip) (Equation 2). It is fit directly from data and has the following intuitive interpretation: $C(D_1) = 0$ when drug 1 does not alter the effect of drug 2, $C(D_1) > 0$ indicates antagonistic interaction, and $C(D_1) < 0$ indicates a synergistic interaction. The one-drug toxicity functions along with $C(D_1)$ accurately describe the entire two-dimensional response surface (right). Circles, experimental measurements; solid lines, nonlinear fits to functional forms in (A); error bars indicate ±1 SE of the growth rate estimate (Supplemental Results). The responses to all 19 drug pairs tested are well described by unidirectional two-drug toxicity functions. See also Figure S2 and Table S5.

(B) Example two-drug toxicity functions $C(D)$ for six different drug pairs. For example, "$C(D)$ for Tmp" (first panel) describes the effects of Cm on trimethoprim (Tmp). Concentrations are measured in units of MIC = K_i for each drug. Ofl, ofloxacin; Tet, tetracycline; Ery, erythromycin.

the amplitude of the two-drug toxicity function $C(D_1)$ (Equation 2) by a single parameter, a_3 (Figure 3). Assumption 1 is consistent with known resistance mechanisms, such as upregulation of efflux pumps (Wood and Cluzel, 2012), enzymatic degradation, and target modification, all of which reduce the effective intracellular concentrations of a drug (Chait et al., 2007). Assumption 2 preserves the shape, but not the magnitude, of the two-drug toxicity function $C(D_1)$. This assumption stems from the idea that new resistant mutants will not fundamentally redefine the strategies that the parent cell has evolved to cope with the stress of specific drugs. There should exist, therefore, a hidden symmetry unifying the responses of drug-sensitive and -resistance cells. Under this assumption, however, the two-drug response surface can still change dramatically—for example, from synergistic to antagonistic—when cells become drug resistant. This change is captured

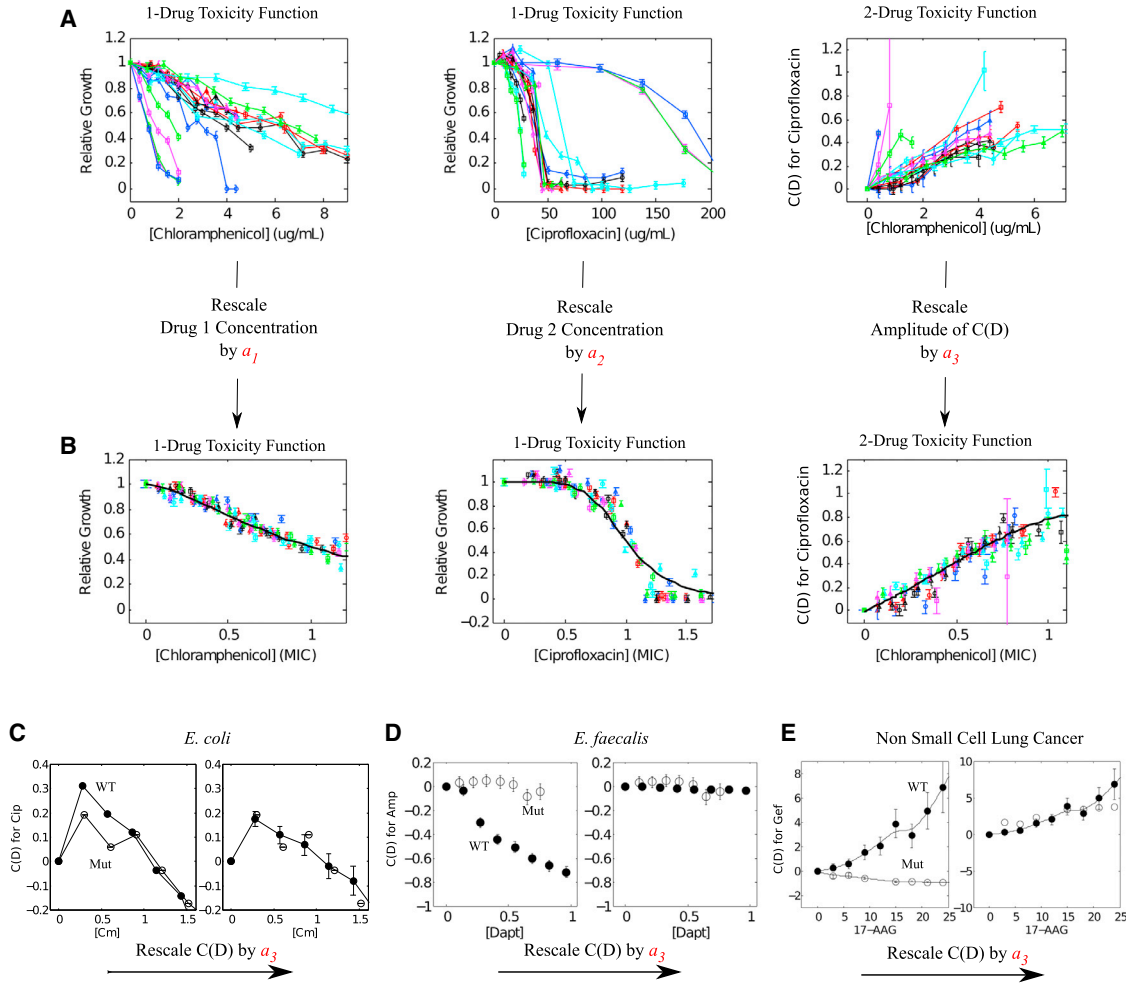

Figure 3. Single-Drug Toxicity Functions and Coupling Functions ($D_{2,eff}/D_2$) for Drug-Resistant Mutants Can Be Rescaled to Match Those in Parental *E. coli*, *E. faecalis*, and NSCLC Cells

(A) Single-drug toxicity functions (top left, top center) and two-drug toxicity functions (top right) for 18 mutant strains isolated by selection in Cm and Cip at various doses (Figure S3; Table S3). Each color/marker combination represents a single mutant. Drug concentrations are in units of μg/ml for Cm (323 g/mol) and ng/ml for Cip (331 g/mol). $C(D_1)$ functions are constructed point by point from raw growth data (Supplemental Results).

(B) One-drug toxicity functions (bottom left, bottom center) and two-drug toxicity functions (bottom right) for all mutant strains are simple rescalings of the corresponding functions in the WT cells (Supplemental Results). A set of three scaling parameters, (a_1, a_2, a_3), provide a set of coordinates that define each mutant. Specifically, mutant one-drug and two-drug toxicity functions are obtained from those of WT cells by applying the following transformations:

$$D_1 \rightarrow D_1' = a_1 D_1$$
$$D_2 \rightarrow D_2' = a_2 D_2$$
$$C \rightarrow C' = a_3 C$$

where a_1, a_2, and a_3 are scaling parameters that describe the change in resistance to drug 1, the change in resistance to drug 2, and the change in the amplitude of $C(D_1)$, respectively, in the resistant mutant. Solid line, bottom: one-drug toxicity functions (left and center) and two-drug toxicity functions (right) that best describe the rescaled data.

(C–E) Examples of rescaling the amplitude of $C(D_1)$ to demonstrate the scaling relations in drug-sensitive and -resistant cells. Left: $C(D_1)$ functions for WT (filled circles) and drug-resistant (open circles) cells. Right: $C(D_1)$ functions for WT (filled circles) and drug-resistant (open circles) cells following a rescaling of the amplitude by a_3. Rescaling of the WT two-drug toxicity (black) Dap C mutant (D; Table S1). Drug concentrations are in units of μg/ml for Cm (323 g/mol), daptomycin (1619 g/mol), and ampicillin (349 g/mol); ng/ml for Cip (331 g/mol); μM for gefitinib (446 g/mol); and nM for 17-AAG (586 g/mol).

In all panels, error bars indicate ±1 SE of the growth rate estimate for toxicity functions (see Supplemental Results) and ±1 SE of the fitted parameter for two-drug toxicity functions.

entirely by the scaling factor a_3. Hypotheses 1 and 2 are further motivated by results from the well-characterized MAR system (Wood and Cluzel, 2012) and by numerical toy models (Supplemental Results). If the model is accurate, it predicts that simple scaling relations establish a quantitative link between the response surfaces of drug-sensitive and -resistant cells. Importantly, this scaling approach implies that it may be possible to predict the full two-drug response of resistant mutants from a

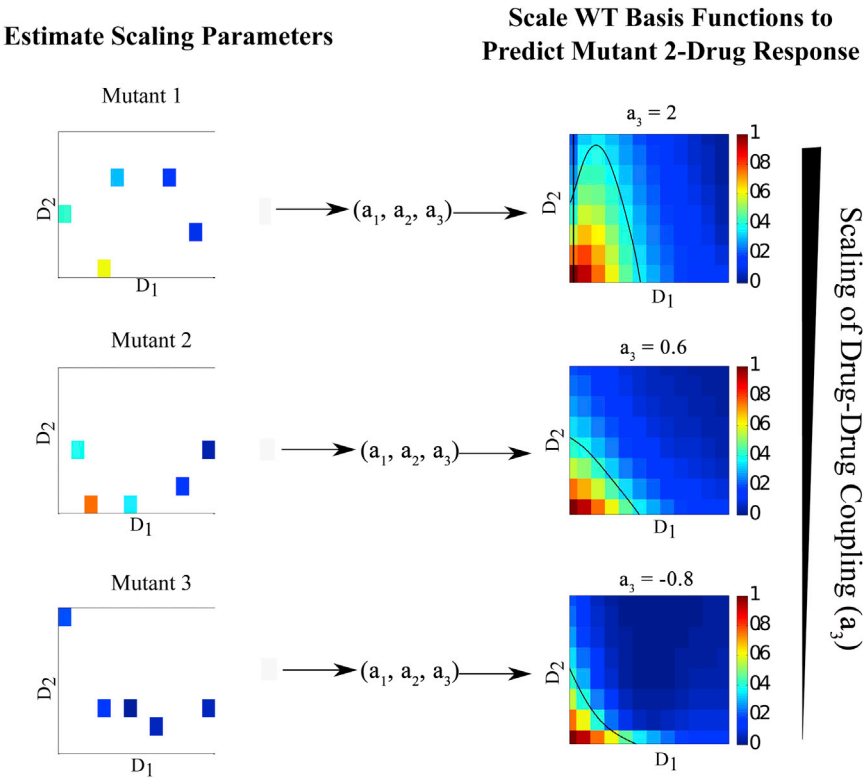

Figure 4. Method for Inferring the Response Surfaces of Drug-Resistant Mutants from the Response Surfaces of WT Cells

The two-drug response surfaces of WT (drug-sensitive) cells can be used to infer the responses of drug-resistant mutants. First, one must extract the three basis functions that describe the WT surface (Figure 2). Second, one can estimate the scaling parameters a_1, a_2, and a_3 using a small number of measurements of the mutant response (left) and then fully reconstruct the response surfaces for each mutant (right).

small number of measurements when the response of drug-sensitive cells is known.

To experimentally test the model, we isolated drug-resistant mutants of *E. coli* by growing WT cells for 30–60 generations in various inhibitory concentrations of Cm and Cip either together or sequentially (see Supplemental Experimental Procedures for experimental details). The concentrations of Cm and Cip were chosen along a single contour of constant growth to keep the conditions of selection approximately constant for all mutants. We then measured the full response surface and extracted the three basis functions that described the effects of the same two drugs (Cm-Cip) on these mutants (Figures 3A, S3A, and S3B). The collection of responses represents a broad range of behaviors, with mutants exhibiting a resistance to Cip and Cm that varies by an order of magnitude or more (Figure 3A, top). However, Figure 3B (bottom) demonstrates that these different behaviors can be unified using a single set of basis functions common to all mutants, and three scaling parameters (a_1, a_2, and a_3) specific to each mutant, thus supporting our scaling hypotheses.

Additionally, we found that this scaling approach was valid for a wide range of cells across several domains of life, including *E. coli*, *E. faecalis*, and human cancer cells (Figures 3C–3E). In some cases, we observed statistically significant (as measured by a_3) small changes in drug interaction, for example, from strongly antagonistic to weakly antagonistic (Figure 3C). In other cases, scaling unified very different phenotypic behaviors, such as the synergy and additivity of ampicillin and daptomycin in WT *E. faecalis* and a daptomycin-resistant (Dap-C) mutant (Figure 3D; see also Figure 1D). Even more surprisingly, scaling laws unified the synergy and antagonism of 17-AAG and gefitinib found in human NSCLC cells and a gefitinib-resistant mutant (Figure 3E; see also Figure 1A). Thus, although response surfaces can sometimes change markedly when resistance is acquired, we find that the functional forms of the underlying basis functions are conserved.

These results suggest that the response surfaces of drug-resistant cells are constrained by those of the drug-sensitive WT cells. If so, one could fully characterize the response surface of a resistant mutant by estimating with only a few measurements the scaling parameters a_1, a_2, and a_3, thus eliminating the need for a labor-intensive sampling of the entire surface. Because this rescaling procedure requires very few measurements, it allows one to infer behavior even in unsampled regions of dosage space (Figure 4, schematic).

Scaling Relations Can Be Used to Rapidly Infer Response Surfaces of Resistant Mutants

To examine whether scaling relations can be used to predict the response surfaces of resistant mutants, we first focused on three clinically relevant bacterial species: *S. aureus*, *E. faecalis*, and *E. coli*. For *S. aureus*, we measured the full response surface of WT and Nor-resistant cells for the drug combination Nor-Cm, which is antagonistic in WT cells (Figure 5A, left; see also Figure 1F). Using only five randomly selected data points, we estimated the scaling parameters and used them to infer mutant growth in unsampled regions of dosage space. The scaling parameters reflect slightly increased sensitivity to Cm ($a_1 > 1$) and increased resistance to Nor ($a_2 << 1$). The antagonism between drugs is equal to that in WT cells ($a_3 \sim 1$; see also Figure 1F), making this example similar to those previously reported in *E. coli* (Figure S3C; Chait et al., 2007).

Next, we compared the responses of a daptomycin-sensitive strain and three daptomycin-resistant strains of *E. faecalis* (Palmer et al., 2011) to combinations of daptomycin and ampicillin (Figures 5B, S4A, and S4B; see also Figure 1D). These strains were evolved under daptomycin pressure and represent three distinct evolutionary routes to daptomycin resistance, each

with a unique set of genetic mutations (Palmer et al., 2011). Using the WT basis functions, we are able to predict the two-drug response for each mutant by estimating the parameters a_1, a_2, and a_3. For the ampicillin-daptomycin combination, all three mutants demonstrate significant resistance to daptomycin ($a_1 < 0.02$), increased sensitivity to ampicillin ($a_2 > 1$), and a drug-drug interaction with slightly ($a_3 = 0.87$, Dap-A mutant) or significantly ($a_3 = 0.05$, Dap-C mutant) decreased synergy (Figure 5B; see also Figure 3D). We also accurately inferred response surfaces for combinations of daptomycin and linezolid, an oxazolidinone that is often used to treat infections of the skin as well as pneumonia (Figures S4C–S4E).

Finally, we tested the scaling hypothesis for two clinically isolated *E. coli* mutants that share a particularly common mechanism of drug resistance: modification of the drug target (Cohen et al., 1989) (748k.01; Figures S4F and S4G). Specifically, each strain exhibited resistance to DNA synthesis inhibitors (fluoroquinolones) arising from distinct mutations in the gene (*gyrA*) encoding the target topoisomerase (Cohen et al., 1989). In both cases, the three-parameter scaling provides an excellent prediction of the response surfaces to Cm and Cip (Figures S4F and S4G), and all mutants exhibit little resistance to Cm ($a_1 \sim 1$), strong resistance to Cip ($a_2 < 0.1$), and significantly weaker drug-drug suppression ($a_3 < 1$) than in the WT. These scaling relationships hold as well for multiple *E. coli* laboratory mutants with evolved resistance to protein synthesis inhibitors, including Dox, Ery, and Cm (Figures S4H–S4K; see also Figures 1B and 1E). We also verified the scaling relations in a cycloheximide-resistant mutant of the budding yeast *Saccharomyces cerevisiae* (Korolev et al., 2012) exposed to a combination of antifungal agents (Figure S4L).

We next asked whether the scaling hypothesis applies to drug combinations targeting human cancer cells, which possess significantly more genetic complexity and redundancy than microbes. Figure 5C shows the previously discussed gefitinib/17-AAG combination, where strong antagonism in the parental NSCLC cells is replaced by synergy in the gefitinib-resistant (GR6) mutant (Engelman et al., 2007). Remarkably, our rescaling approach allows us to predict the mutant response surface for all dosage combinations (see also Figure S4N for the same cells with gefitinib and paclitaxel). We find that there is little resistance to 17-AAG ($a_1 \sim 1$) but a significant increase in gefitinib resistance ($a_2 << 1$). In addition, a_3 switched signs from positive to negative, which accounts for the observed phenotypic change from an antagonistic interaction in the parental cell line to a synergistic interaction in the mutant (recall Figures 1A and 3F). In this case, the synergy arises because 17-AAG inhibits HSP90, which leads to decreased MET protein stability (Xu et al., 2012). The loss of MET, in turn, sensitizes the previously resistant cells to gefitinib. In terms of our scaling model, the gefitinib resistance inverts the drug-drug coupling effect of 17-AAG on gefitinib; rather than lowering the gefitinib toxicity, as in drug-sensitive cells, the presence of 17-AAG raises the effective gefitinib toxicity in mutant cells. These results again demonstrate that the response surfaces can change markedly following the activation of a resistance event, whereas the functional forms of the basis functions are conserved. From a practical perspective, the scaling approach allows us to rapidly recognize the strong synergy between 17-AAG and gefitinib in resistant cells (Figure 5C), and thus identify a potent therapy despite the fact that the drugs are antagonistic in drug-sensitive cells. We also show that the full response surfaces of RAF inhibitor (PLX4720)-resistant melanoma cells to combinations of antineoplastic drugs can be predicted using the same approach (Figure S4M).

Scaling Relations Can Be Used to Increase Potency of Drug Combinations Targeting Cancer Stem Cells

Recent research has also focused on the general drug resistance that appears in cancer stem cells (CSCs), which are believed to underlie the resurgence of many tumors following initial drug treatments (Dick, 2009; Gupta et al., 2009; Reya et al., 2001; Sachlos et al., 2012). Whereas drug-resistant mutants are typically resistant to a small number of specific drugs, CSCs are, in general, more drug resistant than the corresponding cancer cells, and the resistance is not driven by mutations (Dick, 2009; Gupta et al., 2009; Reya et al., 2001; Sachlos et al., 2012). Because of their simultaneous resistance to multiple drugs, CSCs offer an opportunity to test our scaling approach in the context of general drug resistance.

We first directly measured the effects of two anticancer drugs, etoposide and fluorouracil (5-FU), on immortalized human mammary epithelial (HMLE) cells and on matched HMLE populations enriched for mammary CSCs (Gupta et al., 2009). We found that the effects of the individual drugs vary significantly between cell types, with minimum inhibitory concentrations (MICs) increased by factors of ~8.5 for etoposide and ~4 for 5-FU in CSCs. However, the effects of this general drug resistance become more complicated when the drugs are combined. For example, we found that treating the HMLE cells with etoposide and 5-FU at concentrations of 0.35 mM and 1.5 mM, respectively, results in growth inhibition of ~50% (full growth surface shown in Figure 5D, left). One would naively expect a similar inhibition (50%) of CSC growth when the dosages of each drug are increased to account for the increased MICs of the drug individually. However, we measured the inhibitory effects of this naive combination therapy to be only ~20%, which is substantially less than expected. Interestingly, our scaling approach can correctly predict this nonintuitive result with only a few measurements (Figure 5D). Furthermore, the scaling relations predict improved therapies. For example, using 8.5 mM of etoposide alone is correctly predicted to restore growth inhibition to the previous 50% levels (Figure 5D, right). In this case, we are also able to decrease the total amount of drug used, compared with the intuitive therapy. Our prediction quantitatively captures the increased antagonism between 5-FU and etoposide in CSCs, and indicates that scaling relations may be applicable to broadly drug-resistant CSCs.

Overall, we see a wide range of a_3 values from experiments in *E. coli*, *E. faecalis*, *S. aureus*, *S. cerevisiae*, and human cancer cells (Figure S4O), including $a_3 < 0$ (the interaction has changed from antagonistic to synergistic or vice versa), $0 < a_3 < 1$ (the interaction has decreased in magnitude), and $a_3 > 1$ (the interaction has increased in magnitude). In all cases, the mutant response is reconstructed by rescaling the WT basis functions with only three scaling parameters (a_1, a_2, and a_3; Figures 5 and S4A–S4N). Therefore, our scaling hypotheses, which are

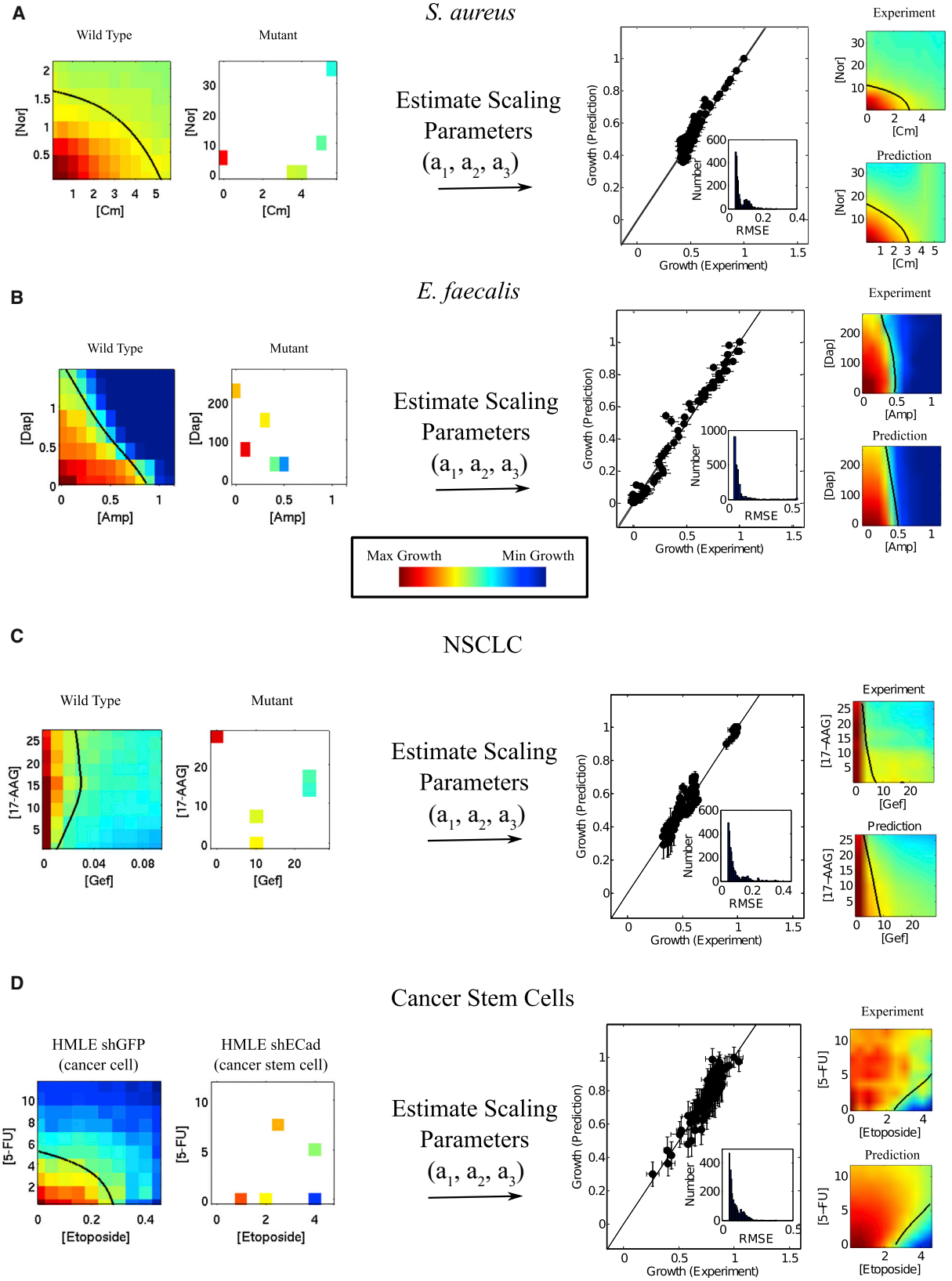

(legend on next page)

based on conservation of basis functions, hold for all resistant cells characterized in this study. The scaling also correctly preserves the interaction (a_3 = 1) in a drug-with-itself mock experiment (Figures S5A–S5D).

Observed Scaling Relationships Are Unlikely to Occur by Chance

In view of the smoothness of the typical drug-response surfaces, it is tempting to think that any two surfaces could perhaps be related by a simple rescaling. Therefore, it is not a priori clear whether the scaling relationships reported here reflect some underlying biological similarity between cellular responses or the scaling relationships are likely to exist between any two-dimensional response surfaces. To explore this question, we developed a null model to quantify the probability of observing our scaling results by chance in a random ensemble of smooth response surfaces (Supplemental Results; Figures S5E and S5F). This analysis reveals that the reported experimental scaling relationships are unlikely to occur by chance ($p < 0.1$ for at least 32 of 42 mutants in the study; Figure S5E). We also find that basis functions from some drug pairs can be rescaled to fit a large number of response surfaces, whereas basis functions from other drug pairs are highly specific to a given drug combination (Figure S5F). Overall, this analysis suggests that the reported scaling relationships do not hold for arbitrary response surfaces and instead represent an unexpected connection between WT and mutant response surfaces. In addition, the scaling approach outperforms standard interpolation methods for predicting growth in unsampled regions of dosage space (Supplemental Results; Figures S5G–S5J) and is robust to variations in how the scaling parameters are determined (Supplemental Results; Figure S5K; Table S7).

Scaling Relations Reflect Species- and Drug-Specific Relationships

To further explore the limits of the observed scaling relationships, we asked whether basis functions derived from one specific bacterial type could be rescaled to infer response surfaces in other bacterial species. As a consequence of hypothesis 2 of the model, it should be possible to use identical basis functions for closely related species because they have most likely evolved similar strategies to cope with chemical stressors. To test this idea, we rescaled the WT basis functions measured for *E. coli* (strain k01.48) exposed to Cm and Cip in an attempt to describe the Cm-Cip response surface in mutants from other bacterial strains. We found that scaled versions of the k01.48 Cm-Cip basis provide an excellent description of drug-resistant mutants from the same strain (Cohen et al., 1989) (k01.48, Figure 6A, red). However, using the same basis functions yields increasingly poor predictions for mutants of more distant *E. coli* strains (Figure 6A, blue) as well as for cells of distantly related bacteria (*E. faecalis*, Figure 6A, black; *S. aureus*, Figure 6A, green). Our results suggest that the scaling relationships may apply across species of closely related organisms, but in general they cannot be used to unify the drug response of distant species.

Similarly, we asked whether the basis functions describing one drug pair could be rescaled to describe the response surface of a different drug pair. For this purpose, we used the basis functions from the Cm-Cip response surface (*E. coli* [BW25113]) to rescale the response surfaces from other drug pairs in the same strain (Figure 6B). We found that the basis functions associated with Cm-Cip provide an excellent model for the response to Cm-ofloxacin (Cm-Ofl), a drug pair with similar modes of action. The same basis also provides a good model for some other drug pairs, such as Cm-lincomycin (Cm-Linc) and Dox-Ofl, whereas other drug pairs, including Cm-trimethoprim (Cm-Tmp) and Ery-Tmp, cannot be well described with the Cm-Cip basis. Interestingly, the shapes of some sets of basis functions are similar, especially when the drugs have similar modes of action. These basis functions may therefore be used to complement existing strategies (Yeh et al., 2006) for functionally classifying drugs because our results indicate that they encode drug-specific information (see also Table S6).

DISCUSSION

We have experimentally shown that the two-drug responses of sensitive and resistant cells share common features unified by simple but general scaling relations. We tested these scaling relations using a broad collection of drugs, including traditional classes of antibiotics (inhibitors of protein synthesis, DNA

Figure 5. Rescaling Parameters Predict the Response of Resistant Mutants to Drug Combinations in Unsampled Regions of Dosage Space

Predicting the response of resistant mutants to a two-drug combination requires estimation of only three scaling parameters if the WT two-drug response is known (see Figure 4).

(A–C) The responses of resistant mutants to each of three two-drug combinations (Cm-Nor in *S. aureus* [A], ampicillin-daptomycin in *E. faecalis* [B], and gefitinib and 17-AAG in NSCLC cells [HCC827] [C]) are predicted using scaling parameters estimated with the WT basis functions and five randomly selected measurements of the mutant's growth rate. Similarly, the responses of drug-resistant CSCs to etoposide and 5-FU are predicted using scaling parameters estimated with the basis functions from parental cells and five randomly selected measurements of the mutant's growth rate. The parameters (a_1, a_2, a_3) describing the mutants, along with SEs, are given by (A) (1.37 ± 0.03, 0.10 ± 0.002; a_3 not needed), (B) (0.88 ± 0.02, 0.017 ± 0.0005, 0.53 ± 0.06), and (C) (a_1, a_2, a_3 = 0.9 ± 0.05, 0.0043 ± 0.0002, −0.22 ± 0.02). Left: heatmap of relative growth rate in WT cells and relative growth rates for five randomly chosen dosages in the mutant cells. Right, large figure: comparison of experiment and prediction for each drug dosage in the mutant cells. Error bars indicate ±SE of prediction. Inset: histograms of root mean-squared error (RMSE) of the predicted two-dimensional mutant growth surfaces constructed from 2,500 independent trials. In each trial, the entire mutant growth surface is predicted using five randomly selected data points on the mutant two-drug surface. Right: heatmaps of relative growth rate for mutant from experiment (top) and prediction (bottom). Black lines show a single contour of constant growth estimated by smoothing the growth surface using cubic spline interpolation (csaps function in MATLAB).

(B–D) The different contour shapes in WT and mutant cells illustrate that drug interactions have changed (see also Figures 1 and S1). Drug concentrations are μg/ml for all drugs except 17-AAG (nM), gefitinib (μM), etoposide (μM), and 5-FU (μM).

Error bars indicate ±1 SE of the growth rate estimate (see Supplemental Results). See also Figure S4.

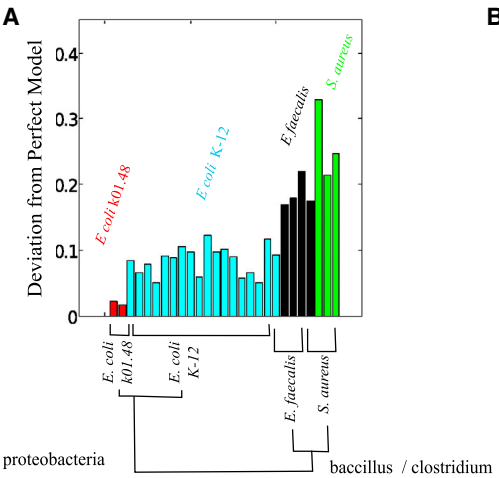

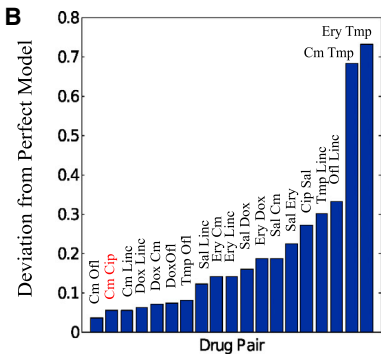

Figure 6. Scaling Relations Hold across Related Species or Drug Classes

(A) The basis functions for Cm and Cip in drug-sensitive *E. coli* (k01.48) are rescaled to fit Cm-Cip response surfaces measured in drug-resistant mutants from the same strain (red) as well as mutants from *E. coli* BW25113 (blue), *E. faecalis* (black), and *S. aureus* (green). Deviation from perfect model is defined as $1 - R^2$, where the coefficient of determination, R^2, is defined as $R^2 = 1 - SS_{err} / SS_{tot}$ (where SS_{err} is the residual sum of squares between model and data, and SS_{tot} is the total sum of squares, which is proportional to the variance of the experimental measurements). A schematic phylogenetic tree is plotted below the horizontal axis.

(B) The basis functions for Cm and Cip in drug-sensitive *E. coli* (BW25113) are rescaled to fit response surfaces to other drug pairs in the same strain. Deviation from perfect model is defined as in (A).

See also Figure S5 for more detailed statistical analysis.

synthesis, cell wall synthesis, and folic acid synthesis), clinically relevant antibiotics (linezolid and daptomycin), and drugs that induce a general stress response (salicylate). We also used both classic chemotherapy drugs (e.g., alkylating agents, microtubule inhibitors, and topoisomerase inhibitors) and targeted therapies. We demonstrated the predictive power of these scaling relations in a wide range of mutants exhibiting many resistance mechanisms, including drug-efflux-mediated resistance, target modification (e.g., fluoroquinolone-resistant *E. coli*; Figures S4F and S4G), pathway reactivation (gefitinib-resistant mutant, as shown in Figures 1A, 3E, and 5C; PLX4720-resistant A375, as shown in Figure S4M), and dedifferentiation (CSCs; Figures 6A and 6B). The scaling relations, analogously to phenomenological laws, are not directly noticeable in two-dimensional response surfaces. However, when the surfaces are decomposed into three basis functions, the underlying symmetry is clear: the shapes of these functions do not change when resistance is acquired. Previous work suggested that interactions between inhibitors of a biochemical network reflect the underlying network topology (Lehár et al., 2007). In our model, these network properties seem to manifest themselves as two-drug toxicity functions with specific functional forms (Supplemental Results). Our primary experimental result is that, surprisingly, these shapes are not fundamentally altered when cells become resistant, even when the response surfaces of drug-sensitive and -resistant cells differ dramatically.

From a molecular perspective, these scaling properties may arise because resistance is conferred by relatively small genetic changes, and not by any major rewiring of intracellular networks that govern the global response to drugs. Therefore, the mutant response is inherently constrained by that of the drug-sensitive parental cells. These scaling relations are evident in genetically similar cells, but they break down when applied across evolutionary distant species. Overall, we found these relationships between drug-sensitive and -resistant cells to be robust within many organisms, both prokaryotic and eukaryotic, and within many classes of drugs. Therefore, scaling relationships may reduce the complexity of drug-resistance studies by unifying the responses of drug-resistant mutants with those of drug-sensitive cells even before specific biochemical mechanisms have been elucidated.

EXPERIMENTAL PROCEDURES

Cell Lines, Strains, and Reagents

Bacteria

The bacterial strains used in this study are listed in Table S1.

Mammalian Cells

HCC827 parental (WT) and gefitinib-resistant (GR6) cells, the latter of which were evolved by stepwise selection in increasing concentrations of gefitinib, were obtained from J. Engelman (Massachusetts General Hospital) and grown in RPMI with 10% fetal bovine serum (FBS) and 1% penicillin/streptomycin. HMLE cells stably expressing lentiviral short hairpin RNAs (shRNAs) against GFP (control) and E-Cadherin were obtained from P. Gupta (Whitehead Institute for Biomedical Research) and grown in media consisting of equal parts of (1) complete MEGM media (Lonza) and (2) Dulbecco's modified Eagle's medium with 10% FBS and 1% penicillin/streptomycin (Gupta et al., 2009). A375 parental (WT) cells were obtained from ATCC and grown in RPMI with 10% FBS and 1% penicillin/streptomycin. PLX4720-resistant A375 cells were engineered by stably overexpressing the kinase C-RAF, which can confer resistance to PLX4720 by overriding B-RAF dependence (Montagut et al., 2008). C-RAF-expressing lentiviruses were produced as previously described (Johannessen et al., 2010; Wood et al., 2012). A375 parental cells were infected at a 1:10 dilution of virus in six-well plates in the presence of 7.5 μg/ml polybrene and centrifuged at 1,200 *g* for 1 hr at 37°C. At 24 hr after infection, blasticidin (10 μg/ml) was added and cells were selected for 72 hr, after which the blasticidin was removed and growth inhibition assays were performed.

Drugs

Drug solutions were made from solid stocks (Table S2). All antibiotic stock solutions were stored in the dark at −20°C in single-use daily aliquots. All drugs were thawed and diluted in sterilized media for experimental use.

Growth-Inhibition Assays

Growth Assay for Bacteria

We inoculated media (LB for *E. coli*, TSB for *S. aureus*, and BHI for *E. faecalis*) from a single colony and grew the cells overnight (12 hr at 30°C with shaking at 200 rpm for *E. coli* and *S. aureus*; no shaking for *E. faecalis*). Following overnight growth, stationary phase cells were diluted (~5,000-fold for *E. coli*

and *S. aureus*; ~1,000-fold for *E. faecalis*) in media. Following the initial dilution, *S. aureus* and *E. faecalis* were grown in drug-free media for 1 hr prior to addition of drugs and transfer to 96-well plates. We transferred *E. coli* to 96-well plates (round bottomed, polystyrene; Corning) immediately following dilution. For each experiment, we set up a two-dimensional matrix of one or two drug combinations in each of four 96-well plates (165–190 μl media per well). For the remainder of the experiment after the addition of drugs (~10–12 hr), cells were grown at 30°C (with shaking at 1,000 rpm on four identical vibrating plate shakers for *E. coli*; no shaking for *E. faecalis*). A_{600} (absorbance at 600 nm, proportional to optical density) was measured at 15–25 min intervals (with one exception; see below) using a Wallac Victor-2 1420 Multilabel Counter (PerkinElmer) combined with an automated robotic system (Twister II; Caliper Life Sciences) to transfer plates between the shakers and the reader. Growth rates in bacteria were determined by fitting background-subtracted growth curves (A_{600} versus time) in early exponential phase ($\sim 0.01 < A_{600} < 0.1$) to an exponential function (MATLAB 7.6.0 curve-fitting toolbox; MathWorks). For *S. aureus* with Nor-Cm (Figure 5), effective exponential growth rates were estimated using background-subtracted A_{600} measurements at times $t = 2$ hr and $t = 6$ hr. True exponential growth curves are therefore not required for this particular assay, which is instead similar to traditional viability assays that compare cell numbers at the end of the experiment (see below). Growth rates were normalized by the growth of cells in the absence of drugs. Error bars, unless otherwise noted, are taken to represent ±1 SE of the fitted parameter.

Growth Assay for Mammalian Cells

Cells were trypsinized, counted, and seeded into 96-well plates at 2,500 cells per well. DMSO or concentrated dilutions of indicated drugs (in DMSO) were added to the cells (1:1,000 in standard media) 24 hr later in otrder to yield the indicated final drug concentrations. Cell viability was measured 4 days after drug addition using the Cell Titer Glo luminescent viability assay (Promega). Viability was calculated as the percentage of control (untreated cells) after background subtraction. Three replicates were performed for each drug/concentration.

Evolved Drug-Resistant Mutants in *E. coli* and *S. aureus*

Drug-resistant *E. coli* mutants were evolved under the conditions listed in Table S3. *S. aureus* Nor-resistant mutants were isolated on Tryptic Soy Agar (BD Biosciences) plates containing 4 μg/ml Nor, followed by spreading of overnight culture of Newman strain.

SUPPLEMENTAL INFORMATION

Supplemental Information includes Supplemental Results, Supplemental Experimental Procedures, five figures, and seven tables and can be found with this article online at http://dx.doi.org/10.1016/j.celrep.2014.02.007.

AUTHOR CONTRIBUTIONS

K.B.W. and P.C. designed the research. K.B.W. performed all experiments in *E. coli* and *E. faecalis*, Cm-Cip experiments in *S. aureus*, and all computational work. K.C.W. designed and performed experiments in human cells. S.N. isolated Nor-resistant *S. aureus* mutants and performed Cm-Nor experiments. K.B.W. and P.C. wrote the manuscript. K.C.W. and S.N. edited the manuscript.

ACKNOWLEDGMENTS

We thank S. Levy for providing *E. coli* 748k0.1, 1-748, and 1-748MM strains; M. Gilmore for *E. faecalis* V583, DapA, DapB, and DapC strains; M. Muller for *S. cerevisiae* cycloheximide-resistant strains; J. Engelman for the gefitinib-resistant HCC827 G6 cells; and P. Gupta for the HMLE cells for CSC experiments. We thank S. Cocco, R. Monasson, E. Sontag, and N. Wingreen for helpful discussions; C. Guet, T. Surrey, and D. Brady for helpful suggestions on the manuscript; K. Dave for editorial assistance; and all members of the P.C. lab for technical guidance and scientific suggestions. The authors are indebted to D. Sabatini, in whose laboratory experiments on human cells were performed. This work was supported in part by National Institutes of Health award P50GM081892-02 to the University of Chicago (to P.C. and S.N.) and National Science Foundation Postdoctoral Fellowship 0805462 (to K.W.).

Received: July 23, 2013
Revised: December 30, 2013
Accepted: February 4, 2014
Published: March 6, 2014

REFERENCES

Balaban, N.Q., Merrin, J., Chait, R., Kowalik, L., and Leibler, S. (2004). Bacterial persistence as a phenotypic switch. Science *305*, 1622–1625.

Bliss, C.I. (1956). The calculation of microbial assays. Bacteriol. Rev. *20*, 243–258.

Bollenbach, T., and Kishony, R. (2011). Resolution of gene regulatory conflicts caused by combinations of antibiotics. Mol. Cell *42*, 413–425.

Bollenbach, T., Quan, S., Chait, R., and Kishony, R. (2009). Nonoptimal microbial response to antibiotics underlies suppressive drug interactions. Cell *139*, 707–718.

Chait, R., Craney, A., and Kishony, R. (2007). Antibiotic interactions that select against resistance. Nature *446*, 668–671.

Cohen, S.P., McMurry, L.M., Hooper, D.C., Wolfson, J.S., and Levy, S.B. (1989). Cross-resistance to fluoroquinolones in multiple-antibiotic-resistant (Mar) Escherichia coli selected by tetracycline or chloramphenicol: decreased drug accumulation associated with membrane changes in addition to OmpF reduction. Antimicrob. Agents Chemother. *33*, 1318–1325.

Dick, J.E. (2009). Looking ahead in cancer stem cell research. Nat. Biotechnol. *27*, 44–46.

Engelman, J.A., Zejnullahu, K., Mitsudomi, T., Song, Y., Hyland, C., Park, J.O., Lindeman, N., Gale, C.M., Zhao, X., Christensen, J., et al. (2007). MET amplification leads to gefitinib resistance in lung cancer by activating ERBB3 signaling. Science *316*, 1039–1043.

Feinerman, O., Veiga, J., Dorfman, J.R., Germain, R.N., and Altan-Bonnet, G. (2008). Variability and robustness in T cell activation from regulated heterogeneity in protein levels. Science *321*, 1081–1084.

Fitzgerald, J.B., Schoeberl, B., Nielsen, U.B., and Sorger, P.K. (2006). Systems biology and combination therapy in the quest for clinical efficacy. Nat. Chem. Biol. *2*, 458–466.

Garrett, J.T., and Arteaga, C.L. (2011). Resistance to HER2-directed antibodies and tyrosine kinase inhibitors: mechanisms and clinical implications. Cancer Biol. Ther. *11*, 793–800.

Glickman, M.S., and Sawyers, C.L. (2012). Converting cancer therapies into cures: lessons from infectious diseases. Cell *148*, 1089–1098.

Greco, W.R., Bravo, G., and Parsons, J.C. (1995). The search for synergy: a critical review from a response surface perspective. Pharmacol. Rev. *47*, 331–385.

Gupta, P.B., Onder, T.T., Jiang, G., Tao, K., Kuperwasser, C., Weinberg, R.A., and Lander, E.S. (2009). Identification of selective inhibitors of cancer stem cells by high-throughput screening. Cell *138*, 645–659.

Jeong, H., Tombor, B., Albert, R., Oltvai, Z.N., and Barabási, A.L. (2000). The large-scale organization of metabolic networks. Nature *407*, 651–654.

Johannessen, C.M., Boehm, J.S., Kim, S.Y., Thomas, S.R., Wardwell, L., Johnson, L.A., Emery, C.M., Stransky, N., Cogdill, A.P., Barretina, J., et al. (2010). COT drives resistance to RAF inhibition through MAP kinase pathway reactivation. Nature *468*, 968–972.

Keith, C.T., Borisy, A.A., and Stockwell, B.R. (2005). Multicomponent therapeutics for networked systems. Nat. Rev. Drug Discov. *4*, 71–78.

Korolev, K.S., Müller, M.J., Karahan, N., Murray, A.W., Hallatschek, O., and Nelson, D.R. (2012). Selective sweeps in growing microbial colonies. Phys. Biol. *9*, 026008.

Lehár, J., Zimmermann, G.R., Krueger, A.S., Molnar, R.A., Ledell, J.T., Heilbut, A.M., Short, G.F., 3rd, Giusti, L.C., Nolan, G.P., Magid, O.A., et al. (2007).

Chemical combination effects predict connectivity in biological systems. Mol. Syst. Biol. *3*, 80.

Lehár, J., Stockwell, B.R., Giaever, G., and Nislow, C. (2008). Combination chemical genetics. Nat. Chem. Biol. *4*, 674–681.

Levy, S.B., and Marshall, B. (2004). Antibacterial resistance worldwide: causes, challenges and responses. Nat. Med. *10* (12, Suppl), S122–S129.

Loewe, S. (1953). The problem of synergism and antagonism of combined drugs. Arzneimittelforschung *3*, 285–290.

Montagut, C., Sharma, S.V., Shioda, T., McDermott, U., Ulman, M., Ulkus, L.E., Dias-Santagata, D., Stubbs, H., Lee, D.Y., Singh, A., et al. (2008). Elevated CRAF as a potential mechanism of acquired resistance to BRAF inhibition in melanoma. Cancer Res. *68*, 4853–4861.

Palmer, K.L., Daniel, A., Hardy, C., Silverman, J., and Gilmore, M.S. (2011). Genetic basis for daptomycin resistance in enterococci. Antimicrob. Agents Chemother. *55*, 3345–3356.

Park, H., Pontius, W., Guet, C.C., Marko, J.F., Emonet, T., and Cluzel, P. (2010). Interdependence of behavioural variability and response to small stimuli in bacteria. Nature *468*, 819–823.

Poulikakos, P.I., and Rosen, N. (2011). Mutant BRAF melanomas—dependence and resistance. Cancer Cell *19*, 11–15.

Rand, K.H., and Houck, H. (2004). Daptomycin synergy with rifampicin and ampicillin against vancomycin-resistant enterococci. J. Antimicrob. Chemother. *53*, 530–532.

Reya, T., Morrison, S.J., Clarke, M.F., and Weissman, I.L. (2001). Stem cells, cancer, and cancer stem cells. Nature *414*, 105–111.

Sachlos, E., Risueño, R.M., Laronde, S., Shapovalova, Z., Lee, J.H., Russell, J., Malig, M., McNicol, J.D., Fiebig-Comyn, A., Graham, M., et al. (2012). Identification of drugs including a dopamine receptor antagonist that selectively target cancer stem cells. Cell *149*, 1284–1297.

Scott, M., Gunderson, C.W., Mateescu, E.M., Zhang, Z., and Hwa, T. (2010). Interdependence of cell growth and gene expression: origins and consequences. Science *330*, 1099–1102.

Shoval, O., Sheftel, H., Shinar, G., Hart, Y., Ramote, O., Mayo, A., Dekel, E., Kavanagh, K., and Alon, U. (2012). Evolutionary trade-offs, Pareto optimality, and the geometry of phenotype space. Science *336*, 1157–1160.

Velenich, A., and Gore, J. (2013). The strength of genetic interactions scales weakly with mutational effects. Genome Biol. *14*, R76.

Wood, K.B., and Cluzel, P. (2012). Trade-offs between drug toxicity and benefit in the multi-antibiotic resistance system underlie optimal growth of E. coli. BMC Syst. Biol. *6*, 48.

Wood, K.C., Konieczkowski, D.J., Johannessen, C.M., Boehm, J.S., Tamayo, P., Botvinnik, O.B., Mesirov, J.P., Hahn, W.C., Root, D.E., Garraway, L.A., and Sabatini, D.M. (2012). MicroSCALE screening reveals genetic modifiers of therapeutic response in melanoma. Sci. Signal. *5*, rs4.

Xu, L., Kikuchi, E., Xu, C., Ebi, H., Ercan, D., Cheng, K.A., Padera, R., Engelman, J.A., Jänne, P.A., Shapiro, G.I., et al. (2012). Combined EGFR/MET or EGFR/HSP90 inhibition is effective in the treatment of lung cancers codriven by mutant EGFR containing T790M and MET. Cancer Res. *72*, 3302–3311.

Yeh, P., Tschumi, A.I., and Kishony, R. (2006). Functional classification of drugs by properties of their pairwise interactions. Nat. Genet. *38*, 489–494.